

Article

Investigating the Zonal Response of Spatiotemporal Dynamics of Australian Grasslands to Ongoing Climate Change

Jingai Bai * and Tingbao Xu 

Fenner School of Environment and Society, Australian National University, Canberra 2601, Australia

* Correspondence: jingai bai66@gmail.com

Abstract: Grasslands are key components of land ecosystems, providing valuable ecosystem services and contributing to local carbon sequestration. Australian grasslands, covering approximately 70% of the continent, are vital for agriculture, pasture, and ecosystem services. Ongoing climate change introduces considerable uncertainties about the dynamic responses of different types of grasslands to changes in regional climate and its variation. This study, bringing together high-resolution meteorological data, calibrated long-term satellite NDVI data, and NPP and statistical models, investigated the spatiotemporal variability of NDVI and NPP and their predominant drivers (temperature and soil water content) across Australia's grassland zones from 1992 to 2021. Results showed a slight, non-significant NDVI increase, primarily driven by improved vegetation in northern savannah grasslands (SGs). Areal average annual NPP values fluctuated annually but with a levelled trend over time, illustrating grassland resilience. NDVI and NPP measures aligned spatially, with values decreasing from the coastal to the inland regions and north to south. Most of the SGs experienced an increase in NDVI and NPP, boosted by abundant soil moisture and warm weather, which promoted vegetation growth and sustained a stable growing biomass in this zone. The increased NDVI and NPP in northern open grasslands (OGs) were linked to wetter conditions, while their decreases in western desert grasslands (DGs) were ascribed to warming and drier weather. Soil water availability was the dominant driver of grassland growth, with NDVI being positively correlated with soil water content but being negatively correlated with temperature across most grasslands. Projections under the SSP126 and SSP370 scenarios using ACCESS-ESM1.5 showed slight NPP increases by 2050 under warmer and wetter conditions, though western and southern grasslands may see declines in vegetation coverage and carbon storage. This study provides insights into the responses of Australian grasslands to climate variability. The results will help to underpin the design of sustainable grassland management strategies and practices under a changing climate for Australia.



Academic Editor: Marko Scholze

Received: 23 December 2024

Revised: 24 January 2025

Accepted: 27 January 2025

Published: 31 January 2025

Citation: Bai, J.; Xu, T. Investigating the Zonal Response of Spatiotemporal Dynamics of Australian Grasslands to Ongoing Climate Change. *Land* **2025**, *14*, 296. <https://doi.org/10.3390/land14020296>

Copyright: © 2025 by the authors. Licensee MDPI, Basel, Switzerland. This article is an open access article distributed under the terms and conditions of the Creative Commons Attribution (CC BY) license (<https://creativecommons.org/licenses/by/4.0/>).

Keywords: Australian grasslands; grassland ecosystem; spatiotemporal distribution pattern; vegetation dynamics; climate change

1. Introduction

Australian grasslands cover approximately 70 percent of the country's surface area [1] and play a significant role in multiple ecological services. In terms of agriculture, grasslands contribute 40% to the gross agricultural production value for Australia [2], provide the major and cheapest feed source for livestock [3], and sustain local food supply and food security [4]. From an ecological conservation perspective, grasslands provide diverse habitats and shelters for various small animal communities [5]. Australian grasslands act

as a terrestrial carbon sink and mitigate climate change both locally and globally [6–10] as they exchange CO₂—a major greenhouse gas—with the atmosphere [11,12] and thereby contribute to stored soil organic carbon [13]. Although grasslands have relatively lower carbon stocks per unit area compared to forest ecosystems, they are major contributors to interannual variations in Australia’s carbon storage. This is due to their vast coverage across Australian landscapes and the high turnover rate of grassland carbon pools [7,8].

The growth, distribution, and function of grassland vegetation are mainly affected by both soil temperature and water [14–16]. Australia—a land of drought and flooding rain—is the driest inhabited continent in the world except for Antarctica, with 70% of arid and semi-arid ecosystems [17]. The Australian climate has warmed by an average of 1.44 ± 0.24 °C since national records began in 1910, with over 1 °C of warming occurring since 1960 [18]. This warming trend leads to higher temperatures, increased summer drying intensity, more frequent heat waves, droughts, and wildfires in Australia [19]. Temperature regulates grassland growth by affecting plant physiology and metabolic reaction rates, such as photosynthesis and respiration [20–22]. The elevated temperatures lead to the decreased soil nutrient availability and thereby reduce vegetation growth and production in grassland ecosystems [23]. Australia exhibits highly fluctuating rainfall regimes, both temporally and spatially [24,25]. Rainfall affects the distribution, growth, and greenness of grassland ecosystems as it modifies the soil moisture available for plant use [26–30]. Precipitable water is an essential component in plant photosynthesis and nutrient transport within the plant [31] and promotes vegetation growth and carbon storage capacity of grassland ecosystems [32–34].

Several studies have examined the growth dynamics of extensive Australian grasslands in response to regional climate patterns. Marchin et al. (2018) found the carbon fluxes in montane grassland in the Snowy Mountains, New South Wales, were limited by temperature despite long growing seasons. Their studies suggested that higher soil temperatures will increase vegetation carbon productivity when the soil water content is unrestricted. Chen et al. (2003) found the net ecosystem production (NEP) in Australian tropical savannahs was overall positive ($3.8 \text{ ton C ha}^{-1} \text{ year}^{-1}$), with a negative value ($-0.2 \text{ ton C ha}^{-1} \text{ season}^{-1}$) in the dry season (May to October) and a positive value (4 ton C ha^{-1} per season) during the wet season (November to April). Their findings revealed savannah growth was tightly coupled with seasonal climate patterns and resultant changes to soil water content and non-limiting temperatures for growth, connecting the seasonal climate dynamics with the grassland growth on a short-term scale. However, the long-term series response of grasslands to climate factors in Australia on an annual scale remains unclear. Rainfall has been shown to have a predominant positive effect on grassland growth in Australia [6,9]; however, these studies focused on the relationship between net terrestrial carbon sink and rainfall rather than the correlation between grassland coverage and soil moisture. Another work [35] explored climate–vegetation interactions in Australian grasslands, focusing on how vegetation responds to climate, with particular emphasis on the increased fire risk associated with climate change. Consequently, there are still research gaps and unanswered questions regarding the zonal response of different types of grasslands to climate dynamics on a national scale, which require further investigation and updating.

Australian grasslands are increasingly impacted by intensified environmental effects [15]. Due to their low stature and sparse coverage, grassland ecosystems are less resilient to climate change and are more vulnerable to complex and unpredictable environmental conditions [19]. Forecast climate change is likely to involve increased rainfall variability, increased uncertainty in water availability, and a greater incidence of high-temperature events, which is exacerbating the increasing loss and fragmentation of grass-

lands in Australia [36]. These impending changes in temperature and soil water availability, along with their consequences for grassland ecosystems, warrant further exploration. Such research can inform projections of grassland dynamics and contribute to effective grassland conservation and management in Australia. Additionally, advanced climate simulations have not been widely used in grassland research, and this area requires further exploration.

Against this background, this study has three aims: (1) to explore spatial–temporal patterns of Australian temperature and soil water content (SWC) during the period of 1992 to 2021; (2) to investigate the growth condition of three grassland zones in Australia by using satellite-based NDVI; (3) to estimate vegetation development across Australian grasslands in response to future climate under the projected emission scenarios by using ACCESS-ESM1.5 in CMIP6. The outcome from this study will provide up-to-date knowledge of Australian grasslands and help improve the policy and strategies for sustainable development and effective management of grassland resources on a national scale.

2. Materials and Methods

2.1. Study Area

This study focused on regions where grasslands are the dominant species in Australia. The grassland map was derived by reclassifying 27 subgroups from the gridded climate classification map of Australia [37], which is available at: <http://www.bom.gov.au/climate/maps/> (accessed on 20 October 2024). The map was established by identifying the classification and distribution of the dominant vegetation types and climate conditions [38]. The grassland cover categories include savannah grasslands (SGs), open grasslands (OGs), and desert grasslands (DGs), respectively (Figure 1).

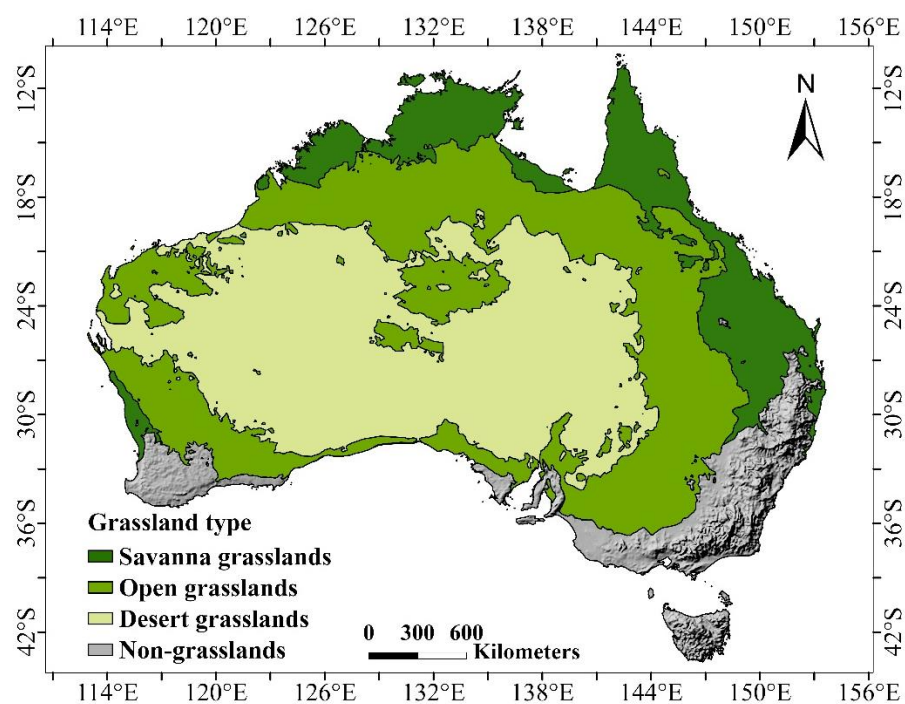


Figure 1. The study area, three major grassland zones in Australia.

The SGs are mostly in northern tropical and subtropical regions of Australia (113.67° E–153.66° E and 10.12° S–33.98° S) where the climate is hot and humid with a predominance of savannahs and grasslands. In the central part of Australia (14.49° S–36.66° S and 112.91° E–149.41° E), the combination of dry seasons and moderate rainfall gives rise to extensive open grasslands that lie between the tropical and temperate zones. The DGs lie in

the driest core of Australia (18.68° S–34.16° S and 113.07° E–144.42° E), where semi-deserts and sparse shrublands dominate over there with scarce rainfall, high temperatures, and a continuous dry condition throughout the year. The southwest and southeast corners of Australia are dominantly covered by croplands and permanent woodlands and were excluded from the scope of this study (grey areas in Figure 1).

2.2. Gridded Meteorological Data

The monthly gridded meteorological data used in this study spanned from 1992 to 2021, with a spatial resolution of 0.01° (approximately 1 km) covering the terrestrial landmass of Australia. This dataset was developed by the Fenner School of Environment and Society of the Australian National University and interpolated from ground-based observations by Xu and Hutchinson [39]. Annual averages were derived from those monthly layers using ArcGIS Pro.

2.3. Temporal Soil Water Content Data from ERA5-Land

This study utilised the fifth-generation global atmospheric reanalysis dataset, ERA5-Land, from the European Centre for Medium-Range Weather Forecasts (ECMWF). ERA5-Land data are derived from high-resolution numerical integrations of the ECMWF land surface model, driven by the downscaled meteorological forcing from the ERA5 climate reanalysis [40]. This global reanalysis dataset provides hourly volumetric soil water content [$\text{m}^3 \text{m}^{-3}$] with a spatial resolution of $0.1^\circ \times 0.1^\circ$. It includes data for 4 soil layers; among them, the second soil layer (7–28 cm depth, “layer 2”) was selected for this study, as the topsoil (0–7 cm, “layer 1”) is more directly influenced by rainfall. Annual averages were derived from hourly layers of this dataset using Python.

2.4. Remote Sensing Normalised Difference Vegetation Index (NDVI) Data

Given the spatial and temporal heterogeneity and variability of grassland coverage, traditional field measurements are not appropriate for large-scale and long-term monitoring of grassland dynamics [41]. The satellite-based normalised difference vegetation index (NDVI) can provide continuous and precise data for monitoring the spatiotemporal pattern of grassland vegetation at a large scale [42]. NDVI, defined as the difference between near-infrared (NIR, 841–876 nm) and red (RED, 620–670 nm) reflectance divided by their sum, using the formula $\text{NDVI} = (\text{NIR} - \text{RED}) / (\text{NIR} + \text{RED})$ [43,44], is a direct indicator used to quantify the greenness, health, and density of vegetation based on satellite remote sensing data [45]. Monthly NDVI with a 0.01° (1 km) spatial resolution from 1992 to 2021 was used for characterising changes in vegetation greenness over time. This dataset, provided by Dr. Tingbao Xu, is a calibrated combination of MODIS Terra NDVI and AVHRR NDVI [46]. Monthly NDVI data were converted to annual averages to investigate the vegetation dynamics of Australian grasslands at different time scales. The annual NDVI was calculated by averaging monthly NDVI for each year.

2.5. Future Climate Scenarios

This study used projected monthly temperature and rainfall datasets for 2050, with a spatial resolution of 0.1°. The datasets were generated using the Australian Community Climate and Earth System Simulator Earth System Model Version 1.5 (ACCESS-ESM1.5) as part of the Coupled Model Inter-comparison Project phase 6 (CMIP6) [47]. Two emission scenarios were selected: shared socioeconomic pathways (SSPs) 126 and SSP370. SSP126 envisions an anthropogenic radiative forcing of 2.6 W/m^2 by 2100 [48], assuming an optimistic scenario where environmentally friendly technologies and renewable energy lead to a green road of sustainable development. SSP370 represents a medium–high level of emission pathway with a radiative forcing of 7 W/m^2 by 2100 [48]. The datasets were

sourced from the National Computational Infrastructure (NCI) platform and are accessible at <https://nci.org.au/> (accessed on 4 October 2024). The projected temperature and rainfall data were used as essential inputs to drive the MIAMI model (details in Section 2.6) for predicting the spatial distribution pattern of NPP for 2050, providing insights into grassland growth conditions in the near future.

2.6. The Miami NPP Model for NPP Estimation

NPP is the difference between the amount of organic carbon fixed by an autotroph through photosynthesis and the amount of carbon lost by their own respiration losses [49,50]. It reflects the net carbon fluxes from the atmosphere into grasslands, which is used for assessing the stability and photosynthetic production capacity of grassland ecosystems [8,51]. The observations of grassland NPP provide valid information on the forage availability and herbivore-carrying capacity at the regional scale [52].

The Miami model is the first global-scale model for terrestrial NPP estimation, which is based on empirical relationships between annual average temperature ($^{\circ}\text{C}$), annual rainfall (mm), and NPP (gC/m^2 per year) [53]. Because of its simplicity and relative accuracy, the model has been widely adopted to calculate the climate-driven potential NPP for large scales [54,55]. The function describing the relationship between rainfall and vegetation productivity is based on the water ratio, where the NPP was observed to increase by 1.0 gC m^{-2} per millimetre of rainfall in arid regions [56]. The function describing the relationship between temperature and vegetation productivity is based on the Van't Hoff rule, where vegetation productivity doubles for each 10°C in the range of -10 – 20°C [56]. The Miami model was used to simulate the NPP across the Australian grasslands from 1992 to 2021 based on ArcGIS Pro software and the ArcPy processing module and was calculated as follows (Equations (1)–(3)):

$$NPP_{T,P} = \min\{f_1(T), f_2(P)\} \quad (1)$$

$$f_1(T) = \frac{3000}{1 + e^{1.315 - 0.119T}} \quad (2)$$

$$f_2(P) = 3000 \left(1 - e^{-0.000664 \times P}\right) \quad (3)$$

where 3000, 1.315, and 0.119 in Equation (2) are the temperature response parameters, and T is the annual average temperature ($^{\circ}\text{C}$); 3000 and 0.000664 in Equation (3) are the rainfall response parameters, and P is the annual average rainfall (mm).

2.7. The Mann–Kendall Trend Analysis

The Mann–Kendall trend test was calculated to determine the overall trends of different variables over time and their reliability, including SWC, temperature, NDVI, and NPP estimates. The Mann–Kendall trend test is a non-parametric test. It is used to statistically assess if there exists a monotonic upward or decreasing trend in long-term sequence variables and has been widely used in meteorological, hydrometeorological, and vegetation productivity studies [57–59].

For a given time series $\{X_i, i = 1, 2, \dots, n\}$, the null hypothesis H_0 assumes that it is independently distributed without a monotonic trend, and the alternative hypothesis H_1 assumes that a monotonic trend is present [59]. The Mann–Kendall trend test examines whether to reject the null hypothesis (H_0) and accept the alternative hypothesis (H_1). The α is the level of the significance test. The significance of the trend can be tested by comparing the value of Z with the critical value α of the desired significance level: when $|Z| \leq Z_{1 - \alpha/2}$, it accepts the null hypothesis, that is, there is no trend with statistical significance; if $|Z| > Z_{1 - \alpha/2}$, it rejects the null hypothesis, that is, there is a trend with

statistical significance. Significance test levels for $|Z| \geq 1.645, 1.960,$ and 2.576 correspond to α being 0.1, 0.05, and 0.01, respectively, which suggest that a temporal series passes 90%, 95%, and 99% of the confidence level of the Mann–Kendall trend test. The formula of the Mann–Kendall trend is calculated as follows (Equations (4)–(7)):

$$S = \sum_{i=1}^{n-1} \sum_{j=i+1}^n \text{sgn}(X_j - X_i) \quad (4)$$

$$Z = \begin{cases} \frac{S-1}{\sqrt{\text{Var}(S)}}, & S > 0 \\ 0, & S = 0 \\ \frac{S+1}{\sqrt{\text{Var}(S)}}, & S < 0 \end{cases} \quad (5)$$

$$\text{sgn}(X_j - X_i) = \begin{cases} +1, & X_j - X_i > 0 \\ 0, & X_j - X_i = 0 \\ -1, & X_j - X_i < 0 \end{cases} \quad (6)$$

$$\text{Var}(S) = [n(n-1)(2n+5)]/18 \quad (7)$$

where X_i and X_j are variables of sequence i, j ; n is the length of the study period (30 years: 1992–2021) in Equation (4); a positive value of Z indicates that the data tend to increase within time series, and conversely, a negative value of Z indicates that the data tend to decrease within time series in Equation (5); $\text{sgn}(X_j - X_i)$ is an indicator function in Equation (6); $\text{Var}(S)$ is the variance of S in Equation (7).

2.8. Pearson Correlation Analysis Between NDVI and Climate Factors

Pearson correlation coefficients were calculated to diagnose the spatial distribution of the relationship between NDVI and two variables (temperature and soil water content). The correlation coefficient ranges from -1 to $+1$. When the correlation coefficient is closer to $-1/+1$, the NDVI and climate variables are better negatively/positively correlated [60]. When it is close to 0, there is no correlation between the climate variables. The ratio of the covariance between the two layers and the product of their standard deviations is called the correlation coefficient. It is a ratio without a unit, and it is calculated as follows (Equations (8)–(10)):

$$\text{Cov}_{ij} = \frac{\sum_{k=1}^N (X_{ik} - \mu_i)(X_{jk} - \mu_j)}{N - 1} \quad (8)$$

$$\sigma = \sqrt{\frac{\sum (X - \mu)^2}{N - 1}} \quad (9)$$

$$\text{Corr}_{ij} = \frac{\text{Cov}_{ij}}{\sigma_i \sigma_j} \in [-1, 1] \quad (10)$$

where Cov_{ij} is the covariance of the variables i and j , σ is the standard deviation of the variables, Corr_{ij} is the correlation coefficient between the two variables, X is the value of a cell, i and j are the two layers of a stack, k denotes a particular cell, X_{ik} is the value of a particular cell k in layer i , μ is the mean of a layer, and N is the number of cells.

2.9. Flow Chart of This Study

Figure 2 is the flow chart of this study.

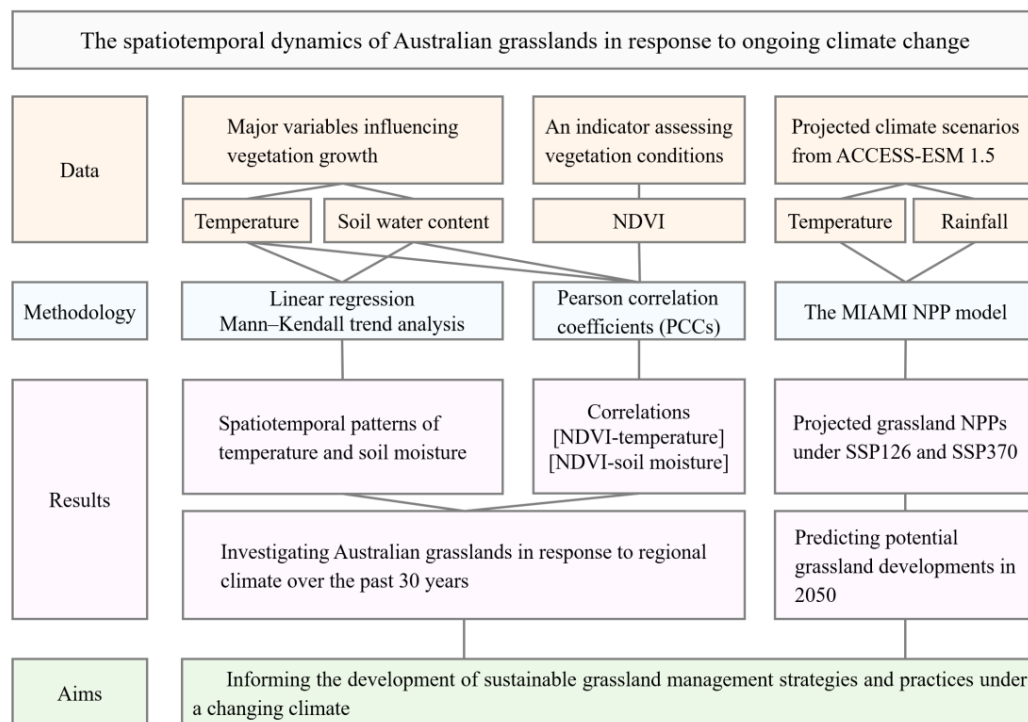


Figure 2. The flow chart of this study.

3. Results

3.1. Meteorological Conditions from 1992 to 2021

The averages of mean annual temperature (MAT) and soil water content (SWC) across Australian grasslands from 1992 to 2021 were 23.01 °C and 0.1785 m³ m⁻³, respectively (Figure 3). MATs exhibited a statistically significant upward trend over the past 30 years ($|Z| = 2.926, p = 0.0034$), whereas SWC did not ($|Z| = 1.428, p = 0.153$). The year 2019 marked the hottest (driest) year, while 2000 was the coldest (wettest) year. Among the grassland zones, SGs had the highest average annual temperature at 24.21 °C, followed by OGs and DGs, with 22.76 °C and 22.79 °C, respectively. The MATs of all three grassland zones, SGs ($|Z| = 2.462, p = 0.0138$), OGs ($|Z| = 2.819, p = 0.0048$), and DGs ($|Z| = 2.926, p = 0.0034$), experienced increasing trends from 1992 to 2021 (Figure 3b). SWC fluctuated considerably across three zones, without a trend exhibited ($|Z| = 0.107$, for SGs). The SGs received the highest annual average water availability (0.2188 m³ m⁻³), followed by OGs (0.1815 m³ m⁻³) and DGs (0.1387 m³ m⁻³) (Figure 3d).

Spatially, MATs decreased from north to south, with the highest temperature observed in northwestern SGs (Figure 4a). Most Australian grasslands have been warming at a rate of 0.2–0.3 °C per decade, except for small areas in the northeast, where a slight cooling was observed (Figure 4b). In the SG and OG regions, the eastern parts experienced stronger warming than the west. The spatial pattern of SWC indicated that eastern grasslands had higher water content than those in the west over the last three decades (see Figure 4c). The highest SWC was found in eastern OGs and SGs, while the lowest SWC was concentrated in the DGs, the arid core of Australia. SWC showed increasing trends in northeastern SGs but decreasing trends across most of the areas in the OGs and DGs (Figure 4d). Notably, a dramatic decrease in SWC was observed in the eastern DGs.

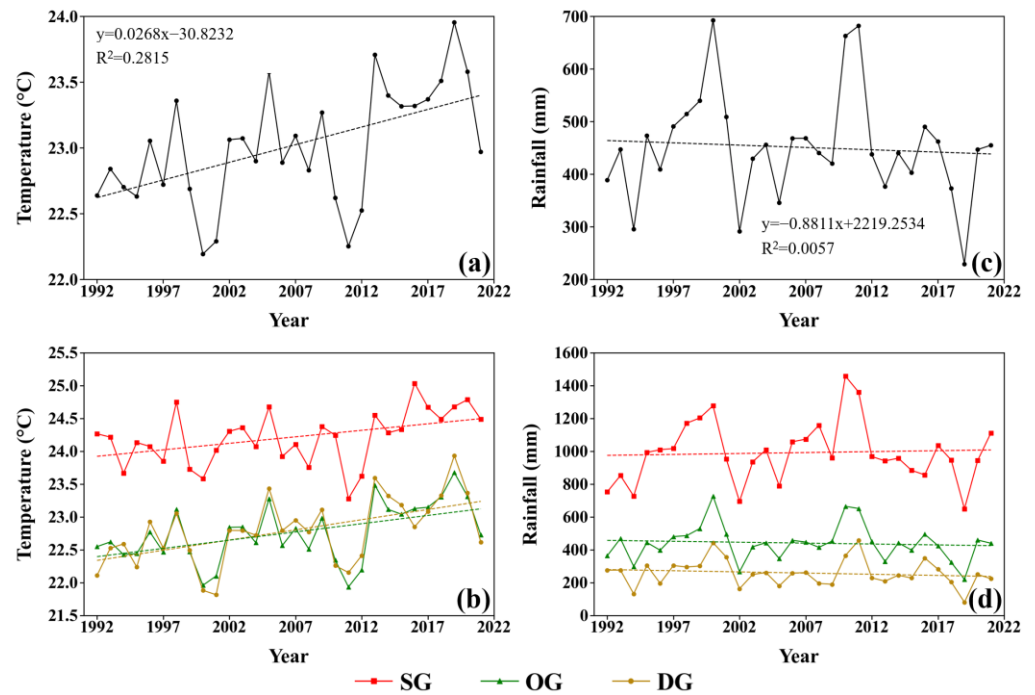


Figure 3. Interannual variations in climate conditions of Australian grasslands and their three zones from 1992 to 2021: MATs (a,b) and SWC (c,d).

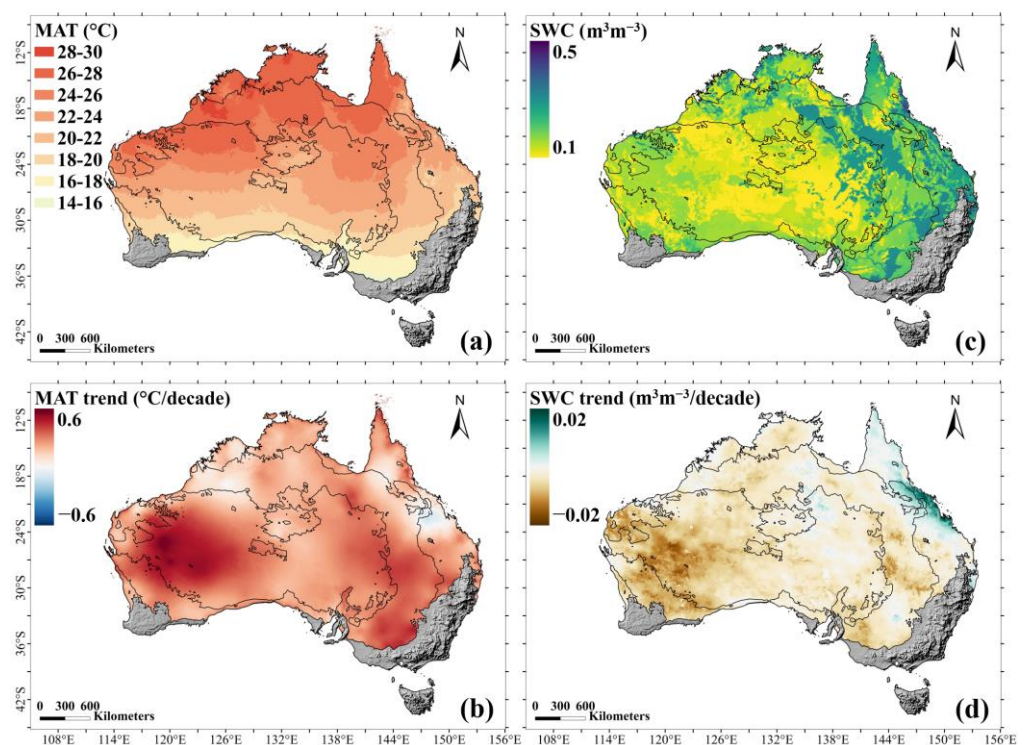


Figure 4. Spatial distributions of annual averages and trends of MATs (a,b) and SWC (c,d) across Australian grasslands from 1992 to 2021. The black contours represent the three grassland zones: SGs, OGs, and DGs, respectively, from north to south. The grey area refers to non-study areas.

3.2. Spatiotemporal Distributions of NDVI and NPP

The mean annual NDVI of Australian grasslands experienced a slight upward trend from 1992 to 2021, though it was not statistically significant ($|Z| = 1.231$, $p = 0.218$) (Figure 5). The highest NDVI was recorded in 2011, while the lowest was observed in 2019, consistent with variations in SWC. NDVI varied notably between the three grassland

zones in Australia owing to the differences in dominant vegetation types and density. SGs, where dense savannahs dominate, had the highest average NDVI (0.338), followed by OGs (0.221), characterised by extensive grasslands, and DGs (0.154), where desert and sparse bush prevail. The mean annual NDVI of SGs experienced a statistically significant increasing trend from 1992 to 2021 ($|Z| = 4.318$), while no such trend was found in OGs ($|Z| = 1.178$) or DGs ($|Z| = 1.499$). Grassland NPP fluctuated considerably, with an average of $719.31 \text{ gC m}^{-2} \text{ yr}^{-1}$ over the last 30 years. Extremely high average annual NPP values were found in 2000 and 2011, while the lowest was recorded in 2019. Although the NPP of Australian grasslands experienced a slight downward trend, it was not statistically significant ($|Z| = 0.535$). SGs had the highest average NPP ($1372.43 \text{ gC m}^{-2} \text{ yr}^{-1}$), followed by OGs ($733.97 \text{ gC m}^{-2} \text{ yr}^{-1}$) and DGs ($462.48 \text{ gC m}^{-2} \text{ yr}^{-1}$).

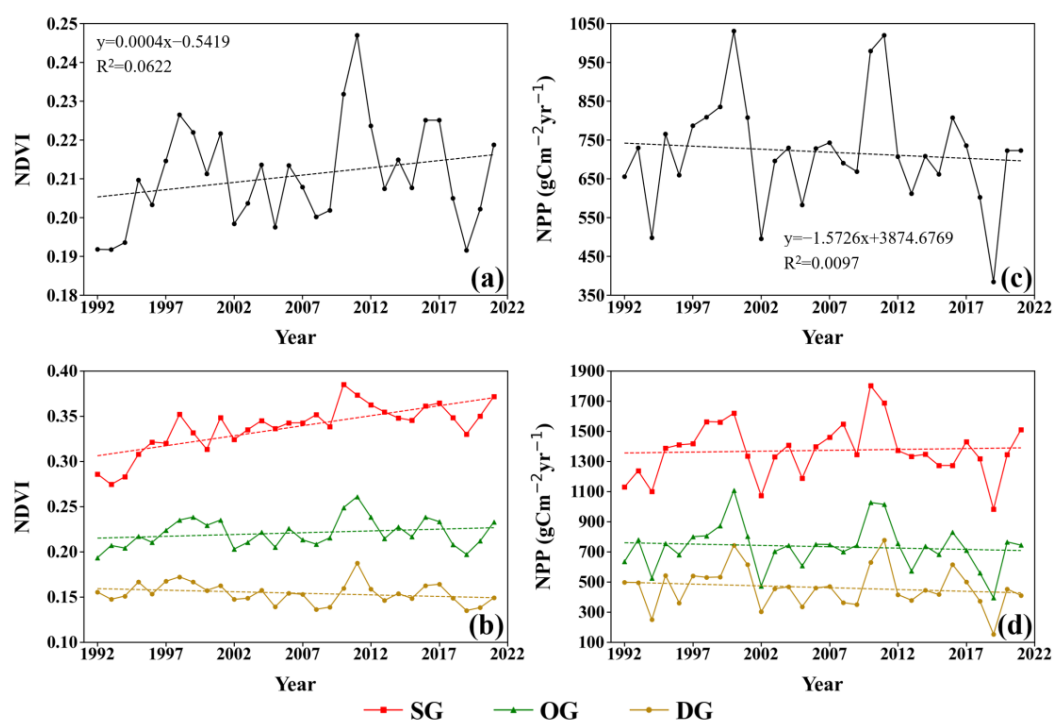


Figure 5. Interannual variations in vegetation condition indicators of Australian grasslands and their three grassland zones from 1992 to 2021: NDVI (a,b) and NPP (c,d).

The mean annual NDVI and NPP exhibited notable spatial consistency across different grassland zones (Figure 6). The spatial distribution of average annual NDVI in Australian grasslands from 1992 to 2021 revealed that northern and eastern coastal regions had higher NDVI values compared to the western coast and inland areas, with the western part of DGs showing higher values than the east. Most of the SGs exhibited an increasing trend in mean annual NDVI (Figure 6b). In DGs, there was a rising NDVI trend in the eastern part, while a declining trend was observed in the central and western parts, generally consistent with the SWC patterns. The spatial distribution of average annual NPP in Australian grasslands indicated that the coastal regions had higher NPP values than inland areas, and northern regions had higher NPP values than southern regions over the past three decades (Figure 6c). The northern part of SGs exhibited the highest NPP, while the interior of Australian grasslands, particularly eastern DGs, had the lowest average annual NPP. The northeast of SGs experienced a remarkable increase in NPP, whereas a decrease was observed in the western parts of DGs and OGs from 1992 to 2021 (Figure 6d).

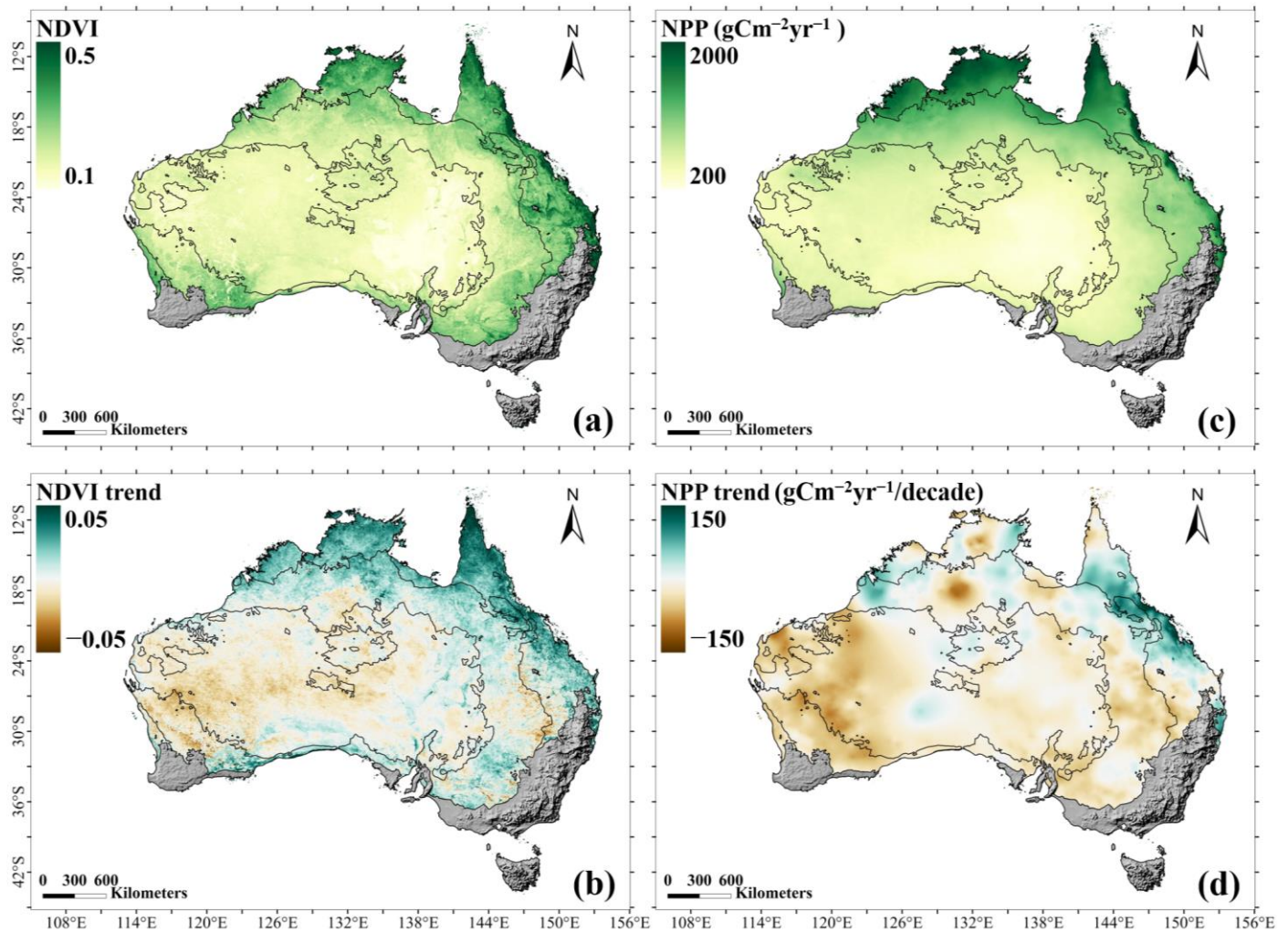


Figure 6. Spatial distributions of annual averages and trends of NDVI (a,b) and NPP (c,d) of Australian grasslands from 1992 to 2021.

3.3. The Relationship Between NDVI and Climate Variables

From 1992 to 2021, the average annual NDVI across Australian grasslands exhibited a negative correlation with temperature (PCCs = -0.3624 , $p < 0.05$) (Table 1). The most pronounced negative correlation between NDVI and temperature was observed in DGs (PCCs = -0.5743 , $p < 0.01$), followed by OGs (PCCs = -0.4576 , $p < 0.05$). Conversely, a positive correlation between NDVI and temperature was identified in SGs (PCCs = 0.1876). In contrast to temperature, the average annual NDVI of Australian grasslands exhibited a statistically significant positive correlation with SWC (PCCs = 0.6748 , $p < 0.01$). The strongest positive correlation between NDVI and SWC was found in DGs (PCCs = 0.7930 , $p < 0.01$), followed by OGs (PCCs = 0.7112 , $p < 0.01$) and SGs (PCCs = 0.4923 , $p < 0.01$).

Table 1. Pearson correlation coefficients between annual mean NDVI and temperature and rainfall across different grassland types during the period of 1992 to 2021.

Grassland Type	NDVI—Temperature	NDVI—SWC
Total Australian grasslands	-0.3624 *	0.6748 **
Desert grasslands (DGs)	-0.5743 **	0.7930 **
Open grasslands (OGs)	-0.4576 *	0.7112 **
Savannah grasslands (SGs)	0.1876	0.4923 **

Note: ** Passed the test at the significance level of 0.01. * Passed the test at the significance level of 0.05.

The spatial correlation coefficient distributions (Figure 7) align with the results presented in Table 1. NDVI exhibited a positive correlation with SWC across most of the grasslands over the past 30 years while showing a negative correlation with temperature, except in the northern coastal regions of SGs.

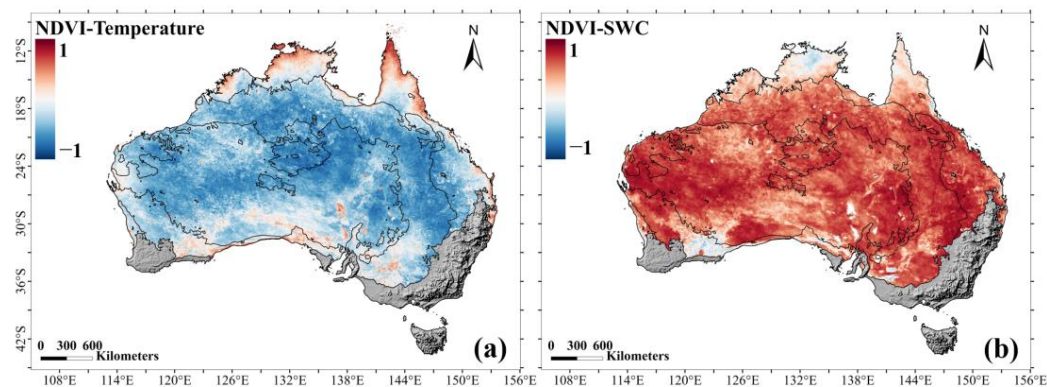


Figure 7. The spatial correlation coefficients between annual NDVI and temperature (a) and soil water content (b) in Australian grasslands from 1992 to 2021.

The significant positive correlation between grassland NDVI and SWC suggested that rainfall was the predominant factor influencing grassland dynamics in Australian grasslands. To further investigate this relationship, the time lag of grassland NDVI in response to rainfall was analysed by calculating PCCs between monthly NDVI and rainfall from 2018 to 2021 across three grassland zones. The time lag was assessed up to two months, covering a total of three months: “no time lag”, “one-month lag”, and “two-month lag” (Table 2). “No time lag” refers to the correlation between rainfall in month N and grassland NDVI in the same month (N); “one-month lag” refers to the correlation between rainfall in month N and NDVI in the subsequent month (N + 1); and “two-month lag” refers to the correlation between rainfall in month N and NDVI two months later (N + 2). The strongest positive correlation occurred when water availability was one month ahead of the NDVI response across all three grassland zones (Table 2).

Table 2. The average monthly PCCs between rainfall and NDVI for three different time lags.

PCCs	DGs	OGs	SGs
No time lag	0.158584	0.334899	0.365565
One-month lag	0.230830	0.438527	0.421997
Two-month lag	0.220880	0.401584	0.389339

3.4. Potential Development of Grasslands Under Future Climate Scenarios

Grassland ecosystems are sensitive and vulnerable to climate fluctuations [4]. To predict future vegetation dynamics and carbon production capacity of Australian grasslands, spatial patterns of temperature and rainfall for 2050 were assessed under two emission scenarios, SSP126 and SSP370, using ACCESS-ESM1.5 simulations in CMIP6. The projected average temperatures for Australian grasslands for 2050 are expected to be 24.68 °C under SSP126 and 24.79 °C under SSP370, which would be warmer by 1.67 °C and 1.78 °C than the average temperature during 1992–2021 (23.01 °C) (Figure 8a,c). In line with historical trends (1992–2021), projected temperatures for 2050 show a gradient decreasing from north to south, with higher temperatures in the northwestern and northern regions. Most Australian grasslands would experience higher temperatures than the 1992–2021 averages, especially in the western, eastern, and southwestern regions.

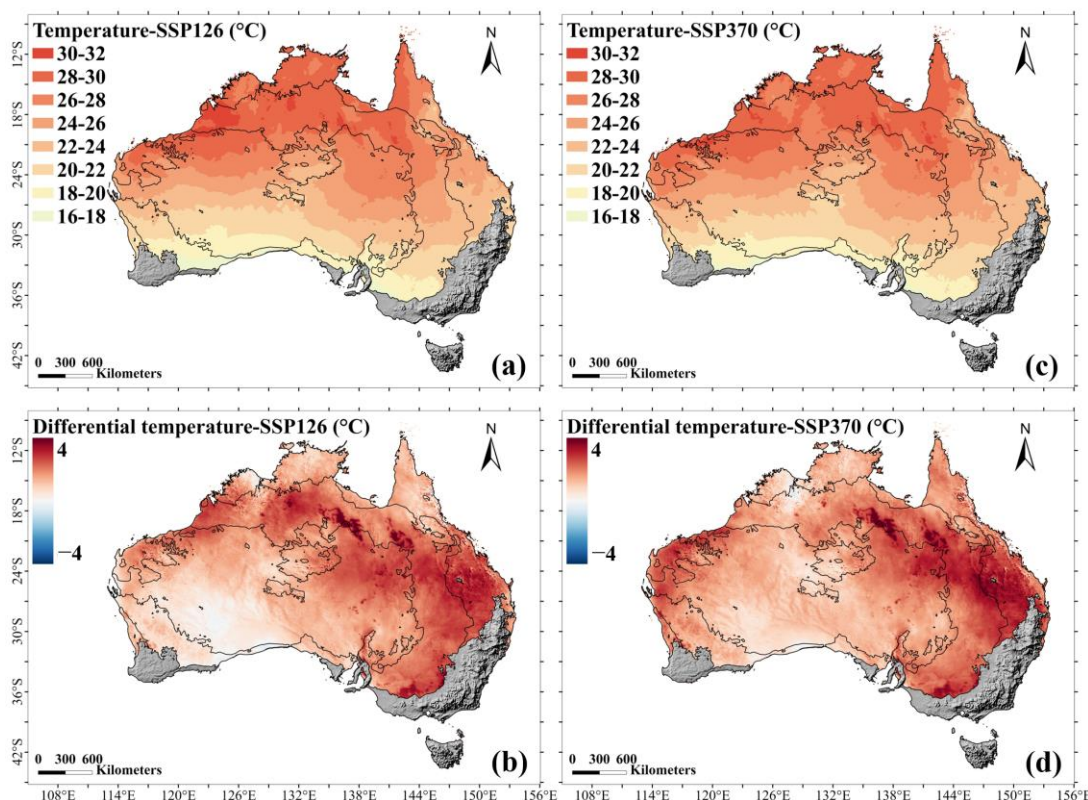


Figure 8. Spatial distributions of projected temperatures across Australian grasslands for 2050 under the SSP126 (a) and SSP370 (c) climate scenarios, as simulated by ACCESS-ESM1.5 in CMIP6. The spatial distribution of temperature differentials between the projected 2050 temperatures and the MATs during 1992–2021 is shown for SSP126 (b) and SSP370 (d) climate scenarios.

The projected rainfall for Australian grasslands for 2050 would be 492.56 mm under SSP126 and 537.25 mm under SSP370, representing increases of 41.11 mm and 85.80 mm, respectively, compared to the rainfall from 1992 to 2021 (451.45 mm) (Figure 9a,c). The spatial pattern of rainfall for 2050 was projected to decrease from the eastern coastal regions to the interior and from northern to southern Australia. Under SSP126, northeastern and central grasslands would receive more rainfall than during 1992–2021, while western and eastern grasslands were going to become drier. Given the ongoing warming in western and eastern grasslands, it was anticipated that vegetation cover may decline in these areas, particularly in eastern SGs and northern and eastern OGs. Under SSP370, northern and eastern grasslands would receive more rainfall compared to the historical records, while southern and western Australia are expected to become drier. Consequently, it was projected that there would be a decline in vegetation coverage in western and southern grasslands. Notably, under both SSP126 and SSP370 scenarios, western grasslands are expected to experience higher temperatures and reduced rainfall compared to 1992–2021, which may negatively impact grassland growth in 2050.

The projected NPP across grasslands for 2050 would be 778.87 $\text{gC m}^{-2} \text{yr}^{-1}$ under SSP126 and 808.02 $\text{gC m}^{-2} \text{yr}^{-1}$ under SSP370, which would be 59.56 $\text{gC m}^{-2} \text{yr}^{-1}$ and 88.71 $\text{gC m}^{-2} \text{yr}^{-1}$ higher than the average annual NPP during 1992–2021 (719.31 $\text{gC m}^{-2} \text{yr}^{-1}$) (Figure 10). Among the three grassland zones, SGs are expected to remain the largest contributor to the local carbon sink in 2050, followed by OGs and DGs, in line with historical patterns during 1992–2021. Under the SSP370 scenario, the potential contribution of southern and western grasslands to the carbon sinks was expected to decline by 2050 due to the increased temperature and reduced rainfall in these regions.

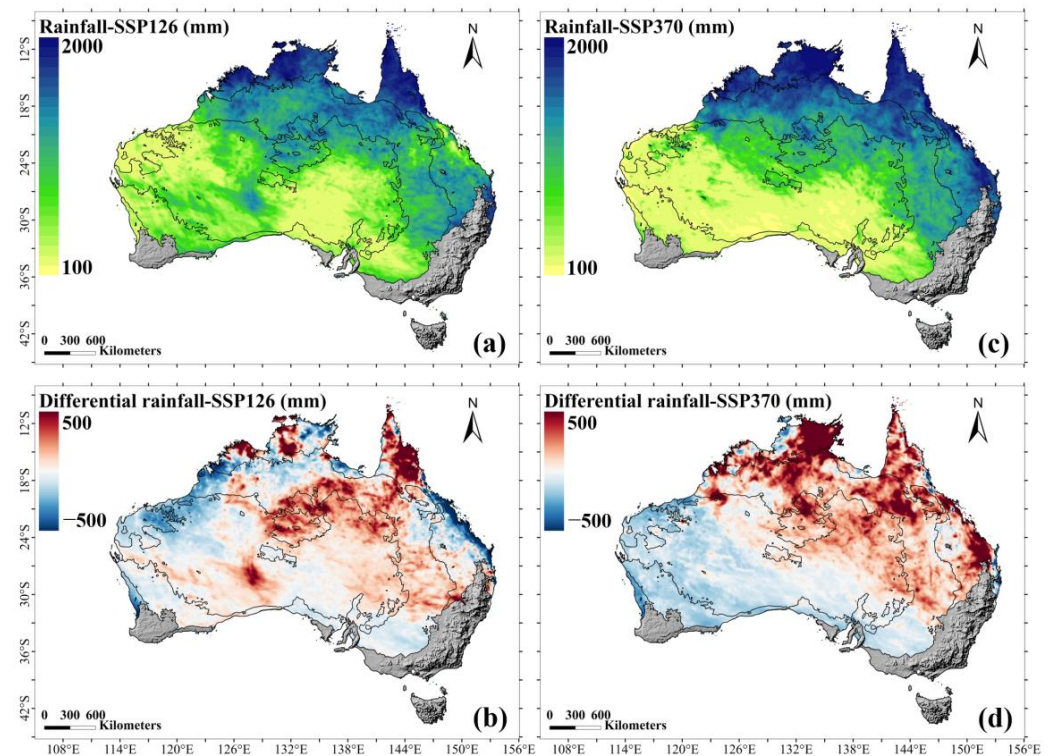


Figure 9. Spatial distributions of projected temperatures across Australian grasslands for 2050 under the SSP126 (a) and SSP370 (c) climate scenarios, as simulated by ACCESS-ESM1.5 in CMIP6. The spatial distribution of rainfall differentials between the projected 2050 rainfall and the rainfall during 1992–2021 is shown for SSP126 (b) and SSP370 (d) climate scenarios.

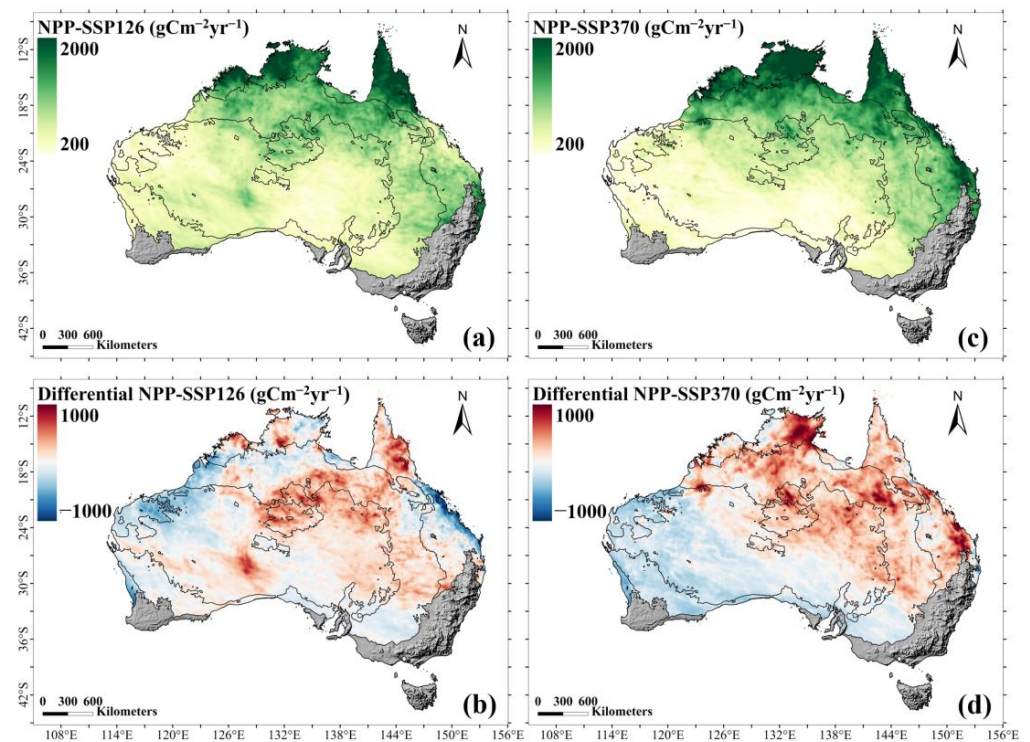


Figure 10. Spatial distributions of projected NPP across Australian grasslands for 2050 under the SSP126 (a) and SSP370 (c) climate scenarios, as simulated by ACCESS-ESM1.5 in CMIP6. The spatial distribution of NPP differentials between the projected 2050 NPP and the mean annual NPP during 1992–2021 is shown for SSP126 (b) and SSP370 (d) climate scenarios.

4. Discussion

4.1. Meteorological Conditions from 1992 to 2021

Temperature and rainfall play a dominant role in affecting plant growth by regulating plant structure and physiological processes [61,62]. Our findings revealed that the inter-annual variability of MATs and SWC varied across the three grassland zones (Figure 3), consistent with an earlier study [63]. From 1992 to 2021, the MATs of Australian grasslands showed an upward trend, aligning with previous findings [64]. Spatially, the MATs in Australia decreased from north to south. Across most of the grasslands, MATs have increased by 0.2–0.3 °C per decade (Figure 4), exceeding the 0.1–0.2 °C rise observed across most of Australia from 1950 to 2000 [65]. The most significant warming occurred in western DGs, largely driven by the enhanced greenhouse effect [66].

The increased SWC in northeastern Australia over the last 30 years indicated a trend towards wetter conditions (Figure 3), primarily driven by the remote influence of low-frequency variations in the El Niño–Southern Oscillation [67]. Northern SGs received the highest rainfall in Australia but did not retain the most soil moisture. In contrast, south-western and southeastern grasslands have become drier over the last three decades, accompanied by warmer temperatures [66]. These observations were closely related to reduced rainfall, driven by changes in the intensity and position of the subtropical ridge [66,68,69], as well as human-induced vegetation clearing for developments [70].

4.2. Spatiotemporal Distributions of NDVI

The remotely sensed NDVI directly reflects both vegetation growth status and coverage, which can be employed for assessing shifts in grasslands over large spatiotemporal scales [71,72]. The analysis revealed a slight upward trend in NDVI during the period of 1992 to 2021 across Australian grasslands (Figure 5a). The highest average annual NDVI was recorded in 2011, aligning with the findings of [10]. Additionally, the spatial pattern of grassland NDVI observed in this study closely corresponds to the NPP patterns reported by [73]. Among the three grassland zones, SGs exhibited the highest NDVI, in agreement with the results of [6,73], despite differences in study periods (Figure 5d). SGs, with their hot and wet climate, supported rich plant species, large plant size, and greater resilience to environmental changes, resulting in a stronger positive response of NDVI and to local climates. Conversely, low NDVI values were observed in OGs and DGs, where hot and dry climates predominated. The OGs and DGs had sparser vegetation density and smaller vegetation sizes, making them less resistant to environmental changes. Both OGs and DGs experienced hotter and drier conditions over the past few decades, leading to weaker vegetation responses to regional climate compared to SGs. However, OGs had a wetter climate and more favourable growing conditions than DGs, leading to higher NDVI levels in OGs than in DGs.

Grassland NDVI exhibited spatial heterogeneity across the three grassland zones, primarily due to variations in water availability and temperature conditions [6] (Figure 6). NDVI displayed a decreasing gradient from coastal to inland regions and from northern to southern Australia, corresponding to the SWC distribution (Figure 6a). This pattern was particularly evident in the eastern grasslands, which received more SWC than the western grasslands and exhibited higher NDVI values compared to the west. The slight increase in NDVI indicated the improved vegetation greenness in SGs (Figure 5b), which is consistent with earlier findings by [10,55]. This trend indicated that the relatively abundant rainfall and warm weather have promoted vegetation growth and maintained stable growing biomass levels over SGs. Additionally, the implementation of vegetation conservation initiatives over the past three decades has reduced vegetation degradation and facilitated the establishment of permanent vegetation in the region. Conversely, the decreased grassland

coverage in western DGs can be ascribed to warming and increasingly arid conditions (Figure 6b).

4.3. The Relationship Between NDVI and Climate Variables

As shown in Table 1, the correlation between average annual NDVI and temperature was negative (-0.3624) from 1992 to 2021 (Table 1). The annual average NDVI was positively correlated with SWC (PCCs = 0.6748) across grasslands, consistent with the findings of [74]. The most significant correlations between NDVI and both temperature and SWC were observed in DGs and OGs, consistent again with the result of [6]. Notably, the average annual NDVI across all grassland zones showed a statistically significant positive correlation with SWC (Table 1), indicating that soil water availability is the primary factor influencing the vegetation status of grassland ecosystems.

The spatial distribution of PCCs (Figure 7) reaffirmed that NDVI was positively correlated with SWC but negatively correlated with temperature across most grasslands. This relationship arises because water availability enhances changes in plant structure, physiological processes, and soil microbiological processes that supply the nutrients necessary for growth [75,76]. Conversely, heat-induced moisture stress diminished plant biomass and photosynthetic activity [76,77], thereby suppressing grassland growth. An exception to this general trend was observed in coastal regions, where NDVI showed a positive correlation with temperature. In these areas, abundant SWC ensured that high temperatures promote grassland growth, as soil water availability is not a limiting factor. This finding was consistent with previous research conducted by [78].

Australian grasslands exhibited a general one-month time lag in response to rainfall across all three grassland zones (Table 2). This finding agrees with the results of [74], who found vegetation NDVI generally lagged one month with respect to soil moisture in most semi-arid ecosystems. This phenomenon can be attributed to the finite time required for both vegetation structure (such as grassland coverage, density, and species composition) and soil structure (such as hydraulic characteristics and nutrient availability) to respond to water supply [52].

4.4. Potential Development of Grasslands Under Future Climate Scenarios

We finally investigated the impact of predicted future temperatures and rainfall for 2050 on Australian grasslands by adopting SSP126 and SSP370 emission scenarios from ACCESS-ESM1.5 in CMIP6 (Figures 8 and 9). Both temperature and rainfall would increase in Australia by 2050 under these scenarios. Grassland NPP for 2050 is also projected to increase slightly compared to the mean annual NPP during 1992–2021 (Figure 10). This slight increase in NPP may be associated with a higher ratio of C4 grasses to C3 grasses due to climate change, as C4 grasses, which fix carbon through a more efficient photosynthesis pathway, are better adapted to hot and dry conditions [79,80].

The temperature and rainfall in 2050 are expected to lead to declines in vegetation coverage and carbon storage capacity in western OGs and DGs. Additionally, increased fluctuations in rainfall events and a higher frequency of climate extremes will contribute to greater fragility and variability in Australia's arid and semi-arid ecosystems in the future [81–83].

From a grassland resource management perspective, the vegetation in western and southern Australian grasslands will be severely threatened by climate change. These regions are particularly vulnerable to rising temperatures and decreasing rainfall, which may lead to reduced grassland coverage and productivity. In response, it is essential to implement appropriate grassland management practices to promote the sustainable development of these vital ecosystems. Such practices include adaptive grazing strategies,

the restoration of native species, and careful monitoring of ecological indicators to ensure the sustainable use of grassland resources amid ongoing environmental changes.

4.5. Limitations and Future Work

More can be carried out to improve this study. Involving more variables in the analysis, apart from temperature and soil moisture, would further strengthen these findings. It is certainly worth fully benefiting from the high quality of climate, soil water content, and NDVI data used in this study and enriching the spatial analysis. In addition, a higher-precision and timely grassland distribution map will boost the practical significance of the results.

5. Conclusions

We assessed the vegetation status of three types of Australian grasslands and their response to a changing climate from 1992 to 2021. The mean annual temperature of the grasslands showed a moderate upward trend, with temperatures in most Australian grasslands increasing by 0.2–0.3 °C per decade, particularly in western and eastern regions. Soil water content (SWC) exhibited large annual fluctuations without a statistically significant trend. Eastern grasslands received more SWC than the western grasslands. Under these climate conditions, grassland NDVI in three grassland zones increased slightly from 1992 to 2021, primarily due to the improved vegetation conditions in the savannah grasslands (SGs). The spatial distribution patterns of NDVI generally declined from north to south and from the coast to the interior, consistent with SWC distribution. High NDVI values were recorded in the SGs, where a hot and wet climate predominates, indicating the abundant soil moisture and warm weather in this zone promoted vegetation growth and sustained stable biomass. The hot and dry conditions in the desert grasslands (DGs) resulted in low and highly variable NDVI. The grassland NDVI was negatively correlated with temperature but positively correlated with SWC across most Australian grasslands. The NDVI exhibited a negative correlation with temperature across most central regions, while a positive correlation was found in the northern coastal areas, where abundant rainfall occurs. This suggests that the suppressive effect of high temperatures on vegetation growth can be mitigated by adequate soil moisture in grasslands. Australian grasslands generally displayed a one-month time lag in response to rainfall across all three zones.

Climate projections under the SSP126 and SSP370 emission scenarios of ACCESS-ESM1.5 in CMIP6 indicated that in the near future, Australian grasslands will experience warmer and slightly wetter conditions. NPP was projected to slightly increase by 2050 compared to the mean NPP from 1992 to 2021. However, the western and southern grasslands were expected to face declines in both vegetation coverage and carbon storage capacity in 2050. This study enhances the understanding of grassland dynamics in Australia under ongoing climate change and provides valuable insights to inform better policymaking in grassland resource management. More efforts could be made to investigate the relationship between grassland conditions and other variables, including solar radiation, soil nutrients and components, and human-induced land changes.

Author Contributions: Conceptualisation, J.B. and T.X.; methodology, J.B. and T.X.; software, J.B.; validation, J.B. and T.X.; formal analysis, J.B.; investigation, J.B.; resources, J.B. and T.X.; data curation, J.B. and T.X.; writing—original draft preparation, J.B.; writing—review and editing, J.B. and T.X.; visualisation, J.B.; supervision, T.X.; project administration, T.X. All authors have read and agreed to the published version of the manuscript.

Funding: This research received no external funding.

Data Availability Statement: Data sharing is not applicable to this article as no new data was created or analysed in this study.

Acknowledgments: We thank data management specialists of the Australian National Computational Infrastructure (NCI) platform for providing assistance in collecting the future climate scenario dataset. We also acknowledge the Commonwealth Scientific and Industrial Research Organisation (CSIRO) for providing the ACCESS-ESM 1.5 dataset used in our analysis and the Australian Bureau of Meteorology for providing the modified gridded Köppen classification map.

Conflicts of Interest: The authors declare no conflicts of interest.

Abbreviations

The following abbreviations are used in this manuscript:

SWC	Soil water content
MAT	Mean annual temperature
SGs	Savannah grasslands
OGs	Open grasslands
DGs	Desert grasslands

References

- McIvor, J.G. Australian grasslands. In *Grasslands of the World*; Suttie, J.M., Reynolds, S.G., Batello, C., Eds.; Food and Agriculture Organization of the United Nations: Rome, Italy, 2005; pp. 343–374.
- Bell, L.W.; Hayes, R.C.; Pembleton, K.G.; Waters, C.M. Opportunities and challenges in Australian grasslands: Pathways to achieve future sustainability and productivity imperatives. *Crop Pasture Sci.* **2014**, *65*, 489–507. [[CrossRef](#)]
- Ali, I.; Cawkwell, F.; Dwyer, E.; Barrett, B.; Green, S. Satellite remote sensing of grasslands: From observation to management. *J. Plant Ecol.* **2016**, *9*, 649–671. [[CrossRef](#)]
- Liu, L.; Sayer, E.J.; Deng, M.; Li, P.; Liu, W.; Wang, X.; Yang, S.; Huang, J.; Luo, J.; Su, Y. The grassland carbon cycle: Mechanisms, responses to global changes, and potential contribution to carbon neutrality. *Fundam. Res.* **2023**, *3*, 209–218. [[CrossRef](#)] [[PubMed](#)]
- Davidson, A.D.; Detling, J.K.; Brown, J.H. Ecological roles and conservation challenges of social, burrowing, herbivorous mammals in the world's grasslands. *Front. Ecol. Environ.* **2012**, *10*, 477–486. [[CrossRef](#)]
- Gang, C.; Zhou, W.; Wang, Z.; Chen, Y.; Li, J.; Chen, J.; Qi, J.; Odeh, I.; Groisman, P. Comparative assessment of grassland NPP dynamics in response to climate change in China, North America, Europe and Australia from 1981 to 2010. *J. Agron. Crop Sci.* **2015**, *201*, 57–68. [[CrossRef](#)]
- Chen, X.; Hutley, L.B.; Eamus, D. Carbon balance of a tropical savanna of northern Australia. *Oecologia* **2003**, *137*, 405–416. [[CrossRef](#)]
- Zhao, M.; Running, S.W. Drought-Induced Reduction in Global Terrestrial Net Primary Production from 2000 Through 2009. *Science* **2010**, *329*, 940–943. [[CrossRef](#)] [[PubMed](#)]
- Haverd, V.; Smith, B.; Trudinger, C. Process contributions of Australian ecosystems to interannual variations in the carbon cycle. *Environ. Res. Lett.* **2016**, *11*, 054013. [[CrossRef](#)]
- Poulter, B.; Frank, D.; Ciais, P.; Myneni, R.B.; Andela, N.; Bi, J.; Broquet, G.; Canadell, J.G.; Chevallier, F.; Liu, Y.Y.; et al. Contribution of semi-arid ecosystems to interannual variability of the global carbon cycle. *Nature* **2014**, *509*, 600–603. [[CrossRef](#)]
- Zhou, W.; Yang, H.; Zhou, L.; Chen, Y.; Huang, L.; Ju, W. Dynamics of grassland carbon sequestration and its coupling relation with hydrothermal factor of Inner Mongolia. *Ecol. Indic.* **2018**, *95*, 1–11. [[CrossRef](#)]
- Stevens, N.; Bond, W.; Feurdean, A.; Lehmann, C.E.R. Grassy Ecosystems in the Anthropocene. *Annu. Rev. Environ. Resour.* **2022**, *47*, 261–289. [[CrossRef](#)]
- Bai, Y.; Cotrufo, M.F. Grassland soil carbon sequestration: Current understanding, challenges, and solutions. *Science* **2022**, *377*, 603–608. [[CrossRef](#)]
- Petermann, J.S.; Buzhdygan, O.Y. Grassland biodiversity. *Curr. Biol.* **2021**, *31*, R1195–R1201. [[CrossRef](#)] [[PubMed](#)]
- Craine, J.M.; Nippert, J.B.; Elmore, A.J.; Skibbe, A.M.; Hutchinson, S.L.; Brunsell, N.A. Timing of climate variability and grassland productivity. *Proc. Natl. Acad. Sci. USA* **2012**, *109*, 3401–3405. [[CrossRef](#)] [[PubMed](#)]
- Xu, H.-j.; Wang, X.-p.; Zhang, X.-x. Alpine grasslands response to climatic factors and anthropogenic activities on the Tibetan Plateau from 2000 to 2012. *Ecol. Eng.* **2016**, *92*, 251–259. [[CrossRef](#)]

17. CSIRO. Australia's Changing Climate. Available online: <https://www.csiro.au/en/research/environmental-impacts/climate-change/State-of-the-Climate/Previous/State-of-the-Climate-2016/Australias-changing-climate> (accessed on 18 September 2023).
18. CSIRO; Bureau of Meteorology. *State of the Climate 2022*; CSIRO: Canberra, Australia, 2021.
19. Gibson, D.J.; Newman, J.A. *Grasslands and Climate Change*; Cambridge University Press: Cambridge, UK, 2019.
20. Gilbert, B.; MacDougall, A.S.; Kadoya, T.; Akasaka, M.; Bennett, J.R.; Lind, E.M.; Flores-Moreno, H.; Firm, J.; Hautier, Y.; Borer, E.T. Climate and local environment structure asynchrony and the stability of primary production in grasslands. *Glob. Ecol. Biogeogr.* **2020**, *29*, 1177–1188. [[CrossRef](#)]
21. Berry, J.; Bjorkman, O. Photosynthetic response and adaptation to temperature in higher plants. *Annu. Rev. Plant Physiol.* **1980**, *31*, 491–543. [[CrossRef](#)]
22. Michaletz, S.T.; Cheng, D.; Kerkhoff, A.J.; Enquist, B.J. Convergence of terrestrial plant production across global climate gradients. *Nature* **2014**, *512*, 39–43. [[CrossRef](#)]
23. Jiao, F.; Shi, X.-R.; Han, F.-P.; Yuan, Z.-Y. Increasing aridity, temperature and soil pH induce soil C-N-P imbalance in grasslands. *Sci. Rep.* **2016**, *6*, 19601. [[CrossRef](#)]
24. Taschetto, A.S.; England, M.H. An analysis of late twentieth century trends in Australian rainfall. *Int. J. Climatol. A J. R. Meteorol. Soc.* **2009**, *29*, 791–807. [[CrossRef](#)]
25. King, A.D.; Klingaman, N.P.; Alexander, L.V.; Donat, M.G.; Jourdain, N.C.; Maher, P. Extreme Rainfall Variability in Australia: Patterns, Drivers, and Predictability. *J. Clim.* **2014**, *27*, 6035–6050. [[CrossRef](#)]
26. Alessandri, A.; Navarra, A. On the coupling between vegetation and rainfall inter-annual anomalies: Possible contributions to seasonal rainfall predictability over land areas. *Geophys. Res. Lett.* **2008**, *35*. [[CrossRef](#)]
27. Guo, Q.; Hu, Z.; Li, S.; Li, X.; Sun, X.; Yu, G. Spatial variations in aboveground net primary productivity along a climate gradient in Eurasian temperate grassland: Effects of mean annual precipitation and its seasonal distribution. *Glob. Change Biol.* **2012**, *18*, 3624–3631. [[CrossRef](#)]
28. Doughty, C.E.; Metcalfe, D.; Girardin, C.; Amézquita, F.F.; Cabrera, D.G.; Huasco, W.H.; Silva-Espejo, J.; Araujo-Murakami, A.; Da Costa, M.; Rocha, W. Drought impact on forest carbon dynamics and fluxes in Amazonia. *Nature* **2015**, *519*, 78–82. [[CrossRef](#)] [[PubMed](#)]
29. Nemani, R.R.; Keeling, C.D.; Hashimoto, H.; Jolly, W.M.; Piper, S.C.; Tucker, C.J.; Myneni, R.B.; Running, S.W. Climate-Driven Increases in Global Terrestrial Net Primary Production from 1982 to 1999. *Science* **2003**, *300*, 1560–1563. [[CrossRef](#)]
30. Reichstein, M.; Bahn, M.; Ciais, P.; Frank, D.; Mahecha, M.D.; Seneviratne, S.I.; Zscheischler, J.; Beer, C.; Buchmann, N.; Frank, D.C.; et al. Climate extremes and the carbon cycle. *Nature* **2013**, *500*, 287–295. [[CrossRef](#)] [[PubMed](#)]
31. Raven, P.H.; Evert, R.F.; Eichhorn, S.E. *Biology of Plants*, 7th ed.; W.H. Freeman and Company: New York, NY, USA, 2005.
32. Cruz-Martínez, K.; Rosling, A.; Zhang, Y.; Song, M.; Andersen, G.L.; Banfield, J.F. Effect of rainfall-induced soil geochemistry dynamics on grassland soil microbial communities. *Appl. Environ. Microbiol.* **2012**, *78*, 7587–7595. [[CrossRef](#)]
33. Gutknecht, J.L.; Field, C.B.; Balsler, T.C. Microbial communities and their responses to simulated global change fluctuate greatly over multiple years. *Glob. Change Biol.* **2012**, *18*, 2256–2269. [[CrossRef](#)]
34. Knapp, A.K.; Smith, M.D. Variation among biomes in temporal dynamics of aboveground primary production. *Science* **2001**, *291*, 481–484. [[CrossRef](#)] [[PubMed](#)]
35. Pitman, A.J.; Narisma, G.T.; McAneney, J. The impact of climate change on the risk of forest and grassland fires in Australia. *Clim. Chang.* **2007**, *84*, 383–401. [[CrossRef](#)]
36. Kane, K.; Debinski, D.M.; Anderson, C.; Scasta, J.D.; Engle, D.M.; Miller, J.R. Using regional climate projections to guide grassland community restoration in the face of climate change. *Front. Plant Sci.* **2017**, *8*, 730. [[CrossRef](#)]
37. Bureau of Meteorology. Climate Classification Maps. Available online: <http://www.bom.gov.au/climate/maps/averages/climate-classification> (accessed on 12 October 2023).
38. Stern, H.; De Hoedt, G.; Ernst, J. Objective classification of Australian climates. *Aust. Meteorol. Mag.* **2000**, *49*, 87–96.
39. Xu, T.; Hutchinson, M.F. New developments and applications in the ANUCLIM spatial climatic and bioclimatic modelling package. *Environ. Model. Softw.* **2013**, *40*, 267–279. [[CrossRef](#)]
40. Muñoz-Sabater, J.; Dutra, E.; Agustí-Panareda, A.; Albergel, C.; Arduini, G.; Balsamo, G.; Boussetta, S.; Choulga, M.; Harrigan, S.; Hersbach, H.; et al. ERA5-Land: A state-of-the-art global reanalysis dataset for land applications. *Earth Syst. Sci. Data* **2021**, *13*, 4349–4383. [[CrossRef](#)]
41. Zhan, C.; Liang, C.; Zhao, L.; Jiang, S.; Niu, K.; Zhang, Y.; Cheng, L. Vegetation Dynamics and its Response to Climate Change in the Yellow River Basin, China. *Front. Environ. Sci.* **2022**, *10*, 892747. [[CrossRef](#)]
42. Zhu, L.; Gong, H.; Dai, Z.; Xu, T.; Su, X. An integrated assessment of the impact of precipitation and groundwater on vegetation growth in arid and semiarid areas. *Environ. Earth Sci.* **2015**, *74*, 5009–5021. [[CrossRef](#)]
43. Weber, D.; Schaepman-Strub, G.; Ecker, K. Predicting habitat quality of protected dry grasslands using Landsat NDVI phenology. *Ecol. Indic.* **2018**, *91*, 447–460. [[CrossRef](#)]

44. Pettorelli, N.; Vik, J.O.; Mysterud, A.; Gaillard, J.-M.; Tucker, C.J.; Stenseth, N.C. Using the satellite-derived NDVI to assess ecological responses to environmental change. *Trends Ecol. Evol.* **2005**, *20*, 503–510. [[CrossRef](#)] [[PubMed](#)]
45. Rhew, I.C.; Vander Stoep, A.; Kearney, A.; Smith, N.L.; Dunbar, M.D. Validation of the Normalized Difference Vegetation Index as a Measure of Neighborhood Greenness. *Ann. Epidemiol.* **2011**, *21*, 946–952. [[CrossRef](#)] [[PubMed](#)]
46. Xu, T. *Technical Report for Project “Improved NDVI data for the National Inventory Report”*; Department of Climate Change, Energy, the Environment and Water: Canberra, Australia, 2022.
47. Mackallah, C.; Chamberlain, M.; Law, R.; Dix, M.; Ziehn, T.; Bi, D.; Bodman, R.; Brown, J.; Dobrohotoff, P.; Druken, K. ACCESS datasets for CMIP6: Methodology and idealised experiments. *J. South. Hemisph. Earth Syst. Sci.* **2022**, *72*, 93–116. [[CrossRef](#)]
48. Meinshausen, M.; Nicholls, Z.R.; Lewis, J.; Gidden, M.J.; Vogel, E.; Freund, M.; Beyerle, U.; Gessner, C.; Nauels, A.; Bauer, N. The shared socio-economic pathway (SSP) greenhouse gas concentrations and their extensions to 2500. *Geosci. Model Dev.* **2020**, *13*, 3571–3605. [[CrossRef](#)]
49. Tum, M.; Zeidler, J.N.; Günther, K.P.; Esch, T. Global NPP and straw bioenergy trends for 2000–2014. *Biomass Bioenergy* **2016**, *90*, 230–236. [[CrossRef](#)]
50. Ma, R.; Xia, C.; Liu, Y.; Wang, Y.; Zhang, J.; Shen, X.; Lu, X.; Jiang, M. Spatiotemporal change of net primary productivity and its response to climate change in temperate grasslands of China. *Front. Plant Sci.* **2022**, *13*, 899800. [[CrossRef](#)] [[PubMed](#)]
51. Sun, J.; Yue, Y.; Niu, H. Evaluation of NPP using three models compared with MODIS-NPP data over China. *PLoS ONE* **2021**, *16*, e0252149. [[CrossRef](#)] [[PubMed](#)]
52. Yahdjian, L.; Sala, O.E. Vegetation structure constrains primary production response to water availability in the patagonian steppe. *Ecology* **2006**, *87*, 952–962. [[CrossRef](#)]
53. Zaks, D.; Ramankutty, N.; Barford, C.; Foley, J.; Zaks, C. From Miami to Madison: Investigating the relationship between climate and terrestrial net primary production. *Glob. Biogeochem. Cycles* **2007**, *21*. [[CrossRef](#)]
54. Ma, J.; Yan, X.; Dong, W.; Chou, J. Gross primary production of global forest ecosystems has been overestimated. *Sci. Rep.* **2015**, *5*, 10820. [[CrossRef](#)]
55. Gao, Q.; Zhu, W.; Schwartz, M.W.; Ganjurjav, H.; Wan, Y.; Qin, X.; Ma, X.; Williamson, M.A.; Li, Y. Climatic change controls productivity variation in global grasslands. *Sci. Rep.* **2016**, *6*, 26958. [[CrossRef](#)] [[PubMed](#)]
56. Lieth, H. Modeling the Primary Productivity of the World. In *Primary Productivity of the Biosphere*; Lieth, H., Whittaker, R.H., Eds.; Springer: Berlin/Heidelberg, Germany, 1975; pp. 237–263.
57. Zhang, Z.; Chang, J.; Xu, C.-Y.; Zhou, Y.; Wu, Y.; Chen, X.; Jiang, S.; Duan, Z. The response of lake area and vegetation cover variations to climate change over the Qinghai-Tibetan Plateau during the past 30years. *Sci. Total Environ.* **2018**, *635*, 443–451. [[CrossRef](#)] [[PubMed](#)]
58. Lin, N.; Li, J.; Jiang, R.; Li, X.; Liu, S. Quantifying the Spatiotemporal Variation of NPP of Different Land Cover Types and the Contribution of Its Associated Factors in the Songnen Plain. *Forests* **2023**, *14*, 1841. [[CrossRef](#)]
59. Wang, F.; Shao, W.; Yu, H.; Kan, G.; He, X.; Zhang, D.; Ren, M.; Wang, G. Re-evaluation of the Power of the Mann-Kendall Test for Detecting Monotonic Trends in Hydrometeorological Time Series. *Front. Earth Sci.* **2020**, *8*. [[CrossRef](#)]
60. Schober, P.; Boer, C.; Schwarte, L.A. Correlation Coefficients: Appropriate Use and Interpretation. *Anesth Analg* **2018**, *126*, 1763–1768. [[CrossRef](#)]
61. Piao, S.; Mohammat, A.; Fang, J.; Cai, Q.; Feng, J. NDVI-based increase in growth of temperate grasslands and its responses to climate changes in China. *Glob. Environ. Change* **2006**, *16*, 340–348. [[CrossRef](#)]
62. Liu, J.; Ji, Y.-H.; Zhou, G.-S.; Zhou, L.; Lyu, X.-M.; Zhou, M.-Z. Temporal and spatial variations of net primary productivity (NPP) and its climate driving effect in the Qinghai-Tibet Plateau, China from 2000 to 2020. *Ying Yong Sheng Tai Xue Bao = J. Appl. Ecol.* **2022**, *33*, 1533–1538.
63. Liu, Y.; Yang, Y.; Wang, Q.; Du, X.; Li, J.; Gang, C.; Zhou, W.; Wang, Z. Evaluating the responses of net primary productivity and carbon use efficiency of global grassland to climate variability along an aridity gradient. *Sci. Total Environ.* **2019**, *652*, 671–682. [[CrossRef](#)]
64. Hughes, L. Climate change and Australia: Trends, projections and impacts. *Austral Ecol.* **2003**, *28*, 423–443. [[CrossRef](#)]
65. Suppiah, R.; Hennessy, K.J.; Whetton, P.H. *Projected Changes in Temperature and Heating Degree-Days for Melbourne, 2003–2007*; Citeseer: Princeton, NJ, USA, 2001.
66. Pitman, A.J.; Narisma, G.T.; Pielke, R.A., Sr.; Holbrook, N.J. Impact of land cover change on the climate of southwest Western Australia. *J. Geophys. Res. Atmos.* **2004**, *109*. [[CrossRef](#)]
67. Sharmila, S.; Hendon, H.H. Mechanisms of multiyear variations of Northern Australia wet-season rainfall. *Sci. Rep.* **2020**, *10*, 5086. [[CrossRef](#)] [[PubMed](#)]
68. Dey, R.; Lewis, S.C.; Arblaster, J.M.; Abram, N.J. A review of past and projected changes in Australia’s rainfall. *Wiley Interdiscip. Rev. Clim. Chang.* **2019**, *10*, e577. [[CrossRef](#)]
69. Whan, K.; Timbal, B.; Lindsay, J. Linear and nonlinear statistical analysis of the impact of sub-tropical ridge intensity and position on south-east Australian rainfall. *Int. J. Climatol.* **2014**, *34*, 326–342. [[CrossRef](#)]

70. Andrich, M.A.; Imberger, J. The effect of land clearing on rainfall and fresh water resources in Western Australia: A multi-functional sustainability analysis. *Int. J. Sustain. Dev. World Ecol.* **2013**, *20*, 549–563. [[CrossRef](#)]
71. Dong, Y.; Yin, D.; Li, X.; Huang, J.; Su, W.; Li, X.; Wang, H. Spatial–temporal evolution of vegetation NDVI in association with climatic, environmental and anthropogenic factors in the loess plateau, China during 2000–2015: Quantitative analysis based on geographical detector model. *Remote Sens.* **2021**, *13*, 4380. [[CrossRef](#)]
72. Guo, M.; Li, J.; He, H.; Xu, J.; Jin, Y. Detecting global vegetation changes using Mann-Kendal (MK) trend test for 1982–2015 time period. *Chin. Geogr. Sci.* **2018**, *28*, 907–919. [[CrossRef](#)]
73. Lin, H.; Feng, Q.; Liang, T.; Ren, J. Modelling global-scale potential grassland changes in spatio-temporal patterns to global climate change. *Int. J. Sustain. Dev. World Ecol.* **2013**, *20*, 83–96. [[CrossRef](#)]
74. Chen, T.; de Jeu, R.A.M.; Liu, Y.Y.; van der Werf, G.R.; Dolman, A.J. Using satellite based soil moisture to quantify the water driven variability in NDVI: A case study over mainland Australia. *Remote Sens. Environ.* **2014**, *140*, 330–338. [[CrossRef](#)]
75. De Dato, G.D.; Pellizzaro, G.; Cesaraccio, C.; Sirca, C.B.; De Angelis, P.; Duce, P.; Spano, D.E.I.; Scarascia Mugnozza, G. Effects of warmer and drier climate conditions on plant composition and biomass production in a Mediterranean shrubland community. *iForest Biogeosci. For.* **2006**, *3*, 511–526. [[CrossRef](#)]
76. WU, Z.; DIJKSTRA, P.; KOCH, G.W.; PEÑUELAS, J.; HUNGATE, B.A. Responses of terrestrial ecosystems to temperature and precipitation change: A meta-analysis of experimental manipulation. *Glob. Change Biol.* **2011**, *17*, 927–942. [[CrossRef](#)]
77. de Valpine, P.; Harte, J. Plant responses to experimental warming in a montane meadow. *Ecology* **2001**, *82*, 637–648. [[CrossRef](#)]
78. Marchin, R.M.; McHugh, I.; Simpson, R.R.; Ingram, L.J.; Balas, D.S.; Evans, B.J.; Adams, M.A. Productivity of an Australian mountain grassland is limited by temperature and dryness despite long growing seasons. *Agric. For. Meteorol.* **2018**, *256–257*, 116–124. [[CrossRef](#)]
79. Sage, R.F.; Monson, R.K.; Ehleringer, J.R.; Adachi, S.; Pearcy, R.W. Some like it hot: The physiological ecology of C4 plant evolution. *Oecologia* **2018**, *187*, 941–966. [[CrossRef](#)]
80. Xie, Q.; Huete, A.; Hall, C.C.; Medlyn, B.E.; Power, S.A.; Davies, J.M.; Medek, D.E.; Beggs, P.J. Satellite-observed shifts in C3/C4 abundance in Australian grasslands are associated with rainfall patterns. *Remote Sens. Environ.* **2022**, *273*, 112983. [[CrossRef](#)]
81. Steffen, W.; Vertessy, R.; Dean, A.; Hughes, L.; Bambrick, H.; Gergis, J.; Rice, M. *Deluge and Drought: Australia’s Water Security in a Changing Climate*; Climate Council: Sydney, Australia, 2018.
82. Myhre, G.; Alterskjær, K.; Stjern, C.W.; Hodnebrog, Ø.; Marelle, L.; Samset, B.H.; Sillmann, J.; Schaller, N.; Fischer, E.; Schulz, M. Frequency of extreme precipitation increases extensively with event rareness under global warming. *Sci. Rep.* **2019**, *9*, 16063. [[CrossRef](#)] [[PubMed](#)]
83. Perkins-Kirkpatrick, S.E.; Lewis, S.C. Increasing trends in regional heatwaves. *Nat. Commun.* **2020**, *11*, 3357. [[CrossRef](#)]

Disclaimer/Publisher’s Note: The statements, opinions and data contained in all publications are solely those of the individual author(s) and contributor(s) and not of MDPI and/or the editor(s). MDPI and/or the editor(s) disclaim responsibility for any injury to people or property resulting from any ideas, methods, instructions or products referred to in the content.